

Two Different Regimes in Alcohol-Induced Coil-Helix Transition: Effects of 2,2,2-Trifluoroethanol on Proteins Being Either Independent of or Enhanced by Solvent Structural Fluctuations

Received 00th January 20xx,
Accepted 00th January 20xx

DOI: 10.1039/x0xx00000x

Hiroyo Ohgi,^a Hiroshi Imamura,^{†b} Tomonari Sumi,^{*c} Keiko Nishikawa,^{a,d} Yoshikata Koga,^e Peter Westh,^f and Takeshi Morita^{*a}

Inhomogeneous distribution of constituent molecules in mixed solvent has been known to give remarkable effects on the solute; e.g. conformational changes of biomolecules in alcohol–water mixture. We investigated general effects of 2,2,2-trifluoroethanol (TFE) on protein/peptide in a mixture of water and TFE using melittin as a model protein. Fluctuations and Kirkwood–Buff integrals (KBIs) in TFE–H₂O mixtures, quantitative descriptions of the inhomogeneity, were determined by small-angle X-ray scattering investigation and compared with those in aqueous solutions of other alcohols. The concentration fluctuation for the mixtures ranks as methanol < ethanol << TFE < *tert*-butanol < 1-propanol, indicating that the inhomogeneity of molecular distribution in TFE–H₂O mixtures is unexpectedly comparable to those of the series of mono-ols. On the basis of the concentration dependence of KBI between TFE molecules, it was found that strong attraction between TFE molecules is not necessarily important to induce the helix conformation, which is inconsistent with the previously proposed mechanism. To address this issue, by combining the KBIs and the helix contents reported by experimental spectroscopic studies, we quantitatively evaluated the change in preferential binding parameter of TFE to melittin attributed to the coil-helix transition. As a result, we found two different regimes on TFE-induced helix formation. In the dilute concentration region of TFE below ~2 M, where the TFE molecules are not aggregated among themselves, the excess preferential binding of TFE to the helix occurs due to the direct interaction between them, namely independent of the solvent fluctuation. In higher concentrations than ~2 M, in addition to the former effect, the excess preferential binding is significantly enhanced by the solvent fluctuation. This scheme should be held as general cosolvent effects of TFE on protein/peptide.

1. Introduction

2,2,2-Trifluoroethanol (TFE) has a marked ability to induce structural changes in various proteins and peptides in an aqueous solution. For instance,¹ although TFE–H₂O and ethanol–H₂O mixtures have almost the same dielectric constant, the necessary volume fraction of TFE at which the solution induces α -helix in bovine β -lactoglobulin and melittin is less than half of that of ethanol.

Effects of alcohols on biomolecules have been investigated since the 1950s.^{2,3} In the 1950s, α -helical structures were assumed to be present naturally.² Hence, Doty *et al.*² tried to reproduce the α -helical configuration of proteins in a peptide using copoly-L-lysine-L-glutamic acid as a model peptide. They found 2-chloroethanol to be effective in inducing α -helix in the peptide. Later, Weber and Tanford⁴ measured structural transition of a protein, ribonuclease by addition of 2-chloroethanol. It was also found that other alcohols such as methanol, ethanol, 1-propanol, and 1-butanol have the function of the α -helix induction, and the same is true for other organic cosolvents.⁵ TFE was effective in inducing α -helical structure in ribonuclease S-peptide, as the S-peptide undergoes the coil-helix transition in its binding process.⁶

The trend has changed from mimicking α -helix to investigating the mechanisms of proteins' folding since the late 1960s. To see the effect of the solvent perturbation on protein folding, cosolvents or cosolutes, not only TFE but also Na₂SO₄, guanidine hydrochloride, and dimethyl sulfoxide and so on were utilized.^{7,8}

Since the 1980s, the marked ability of TFE to stabilize the α -helix has attracted much attention. The effects of TFE on biomolecules were extensively investigated using a variation of concentration of TFE and temperature.^{9,10} Debates on the

^a Department of Chemistry, Graduate School of Science, Chiba University, Chiba 263-8522, Japan

^b Department of Applied Chemistry, College of Life Sciences, Ritsumeikan University, Shiga 525-8577, Japan

^c Research Institute for Interdisciplinary Science, Okayama University, Okayama 700-8530, Japan.

^d Toyota Physical & Chemical Research Institute, Nagakute, Aichi 480-1192, Japan

^e Department of Chemistry, The University of British Columbia, Vancouver, Canada V6T 1Z1

^f Department of Biotechnology and Biomedicine, Technical University of Denmark, Søtofts Plads, 2800, Kgs. Lyngby, Denmark

[†] HO and HI contributed equally.

*Corresponding authors.

E-mail: sumi@okayama-u.ac.jp (T. Sumi); moritat@faculty.chiba-u.jp (T. Morita)

Electronic Supplementary Information (ESI) available: [details of any supplementary information available should be included here]. See DOI: 10.1039/x0xx00000x

molecular mechanisms for this effect started in the 1990s. Although TFE has a low dielectric constant, Hong *et al.*¹ pointed out a limitation of the explanation using such a macroscopic feature of TFE–H₂O mixture. In the literature, the suggestion to explain the effect of TFE is cluster formation of TFE molecules, which provides a locally low polarity region to proteins and peptides.¹ Small-angle X-ray scattering from TFE–H₂O mixture has been interpreted in support of the clustering.^{1,11} Another proposal is based on the concept of preferential binding of TFE to proteins or peptides.¹⁰ Such discussion has been progressed further by theoretical studies.^{12,13} Westh and Koga have suggested that the effect of TFE on H₂O in the lower TFE concentration, where TFE molecules would not form so-called clustering or aggregated structure, is could be responsible: H₂O mediated enthalpic lysozyme-alcohol interaction was clarified to be unfavorable.^{14,15} Dependence of helix induction on the solution structure of TFE–H₂O mixture at different TFE concentrations is still unclear because of lack of detailed information on solvent fluctuations, *e.g.*, molecular aggregation of TFE in water.

Some applications of TFE–H₂O mixtures have been reported. The effects of TFE on the formation of amyloid fibrils have been investigated.^{16,17} Intermolecular potential between protein molecules in aqueous TFE solution was measured using scattering methods.^{18,19} TFE was used as a model of the hydrophobic membrane.^{20,21} Understanding the characteristics of TFE–H₂O mixtures, which provides such functional environment to biomolecules, is fundamentally important. In addition, the conformation of proteins in TFE–H₂O resembles an intermediate prone to aggregate.¹⁹ Therefore, the study of TFE–H₂O mixtures has the potential to elucidate the mechanisms of aggregation.

Investigations focusing on TFE–H₂O mixtures using molecular dynamics (MD) simulation,^{22–25} Fourier transform infrared (FTIR) spectroscopy and nuclear magnetic resonance (NMR)²⁶ were employed to understand the structure of the mixture. It is reported from MD simulation that the ratio of the number of molecules of TFE and H₂O in a sphere of 3 nm radius in 40%(v/v) (0.14 mole fraction of TFE, x_{TFE}) TFE at 25 °C fluctuates in the order of nanoseconds.²² From the FTIR and NMR studies, it was found that hydrogen bond probability between H₂O molecules is decreased in the concentration region of $x_{\text{TFE}} \geq 0.3$, while the strength of the hydrogen bond appears not to change compared to that for the more dilute composition region at 25 °C.²⁶

The present research attempts at investigating the effect of TFE as a typical example of the effect of alcohols on biomolecules from the viewpoint of the characteristics of TFE–H₂O mixture as a solvent. Here, we determined the inhomogeneity of molecular distribution of the TFE–H₂O mixture using the small-angle scattering method. On the basis of the determined structural fluctuations, preferential binding of TFE molecules induced by the large inhomogeneity of the mixing state was quantitatively evaluated as the difference between the coil and the helix conformations of protein in the TFE–H₂O system toward understanding TFE-induced helix formation of proteins and peptides.

Small-angle scattering method of X-rays and neutron is a powerful tool for evaluation of mixing state and inhomogeneity of molecular distribution in solution systems. The method provides structural information in nano and mesoscopic length scales complementarily to large-angle scattering,²⁷ which gives microscopic information such as radial distribution function. Kuprin *et al.*¹¹ and Hong *et al.*¹ observed sharply increased scattering at TFE concentrations of 30–40%(v/v) ($x_{\text{TFE}} = \text{ca. } 0.096\text{--}0.14$). They interpreted the result as the existence of micelle-like clusters in TFE–H₂O mixture in this concentration region. An approach to give more decisive information on the structural fluctuations in molecular distribution and aggregation has been derived using the small-angle scattering method.^{28–30} The fluctuation parameters are defined as particle number fluctuations,²⁸ the Kirkwood-Buff integrals (KBIs),³¹ and density fluctuations for each component.^{32,33} Previously, we have determined the fluctuations of two-component systems^{30,33–39} and supercritical fluids.^{40–42} In the present research, to clarify the effect of TFE on biomolecules, we applied the small-angle scattering method to TFE–H₂O mixture and precisely determined the KBIs.

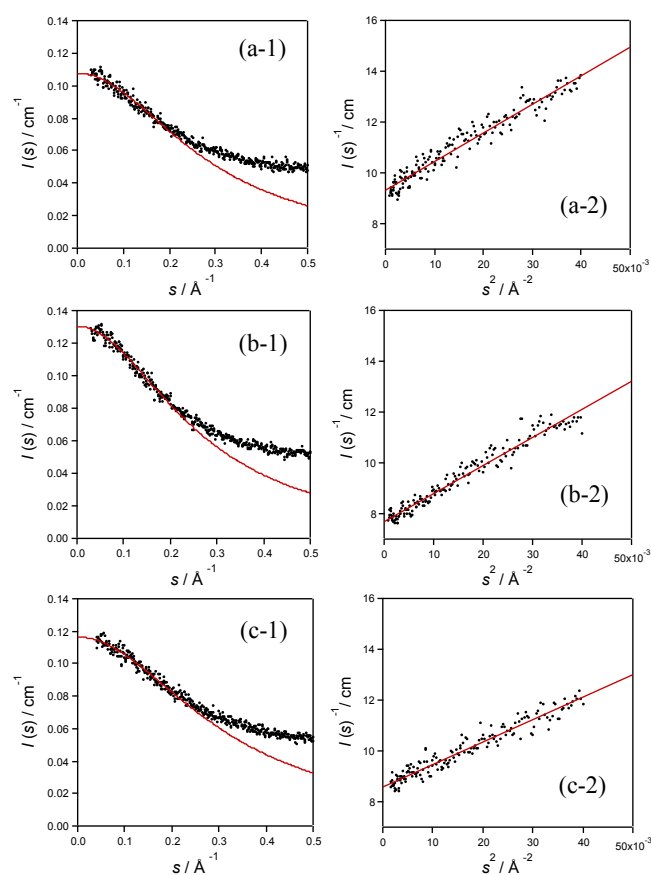


Figure 1. SAXS profiles (black dots) and the Ornstein-Zernike plots (red lines) of TFE–H₂O mixtures at 25.0 °C in the absolute scale for typical TFE mole fractions at (a) $x_{\text{TFE}} = 0.09994$, (b) $x_{\text{TFE}} = 0.1372$, and (c) $x_{\text{TFE}} = 0.1857$, around which concentration dependence of the SAXS intensities takes maximum.

The concept “fluctuation” is fruitful for representing an inhomogeneity of molecular distribution and mixing state of solution systems. We also use the terms “aggregation” and “cluster” for describing a large structural fluctuation in TFE solution; the fluctuation is a quantitative representation of the molecular distribution of solvent, cosolvent, and their correlations.

Goto and colleagues proposed the following principal molecular mechanism on the remarkable ability of TFE-induced helix formation of proteins and peptides: (1) a direct interaction between TFE and proteins should be stronger than that between the other mono-ols and the proteins,^{43,44} and (2) low polar region locally created by a larger solvent structural fluctuation of TFE–H₂O mixtures is favorable for formation of the helix.¹ However, it remains unclear that these mechanisms work collaboratively or independently. To address this issue, we presented a general thermodynamic description on conformational transition of proteins and peptides in terms of the excess preferential binding of TFE to the helix (versus the coil). The excess preferential binding is incorporated with the evaluated KBIs, the helix content reported by circular dichroism (CD) studies,^{43,44} and a preferential binding theory proposed by Smith *et al.*^{45,46} The effects include the solvent fluctuation and molecular distribution in each component. The present results show that two different regimes are both relevant, but their importance depends on the TFE concentration. We also demonstrate that the molecular mechanism proposed here represents the general cosolvent effects of TFE on peptides and proteins.

2. Experimental

TFE (Fluorochem Ltd, UK, 99%) was used as supplied. The sample solutions were gravimetrically prepared by mixing the ultrapure water of Milli-Q system (EMD Millipore, MA).

2.1 SAXS.

SAXS measurements were carried out using laboratory X-ray source and synchrotron radiation to carefully check the repeatability and traceability of the scattering measurements. The results of SAXS data were reproduced with each other in the error of less than 5%.⁴⁷ The scattering profiles were converted to the absolute scale on the basis of the zero-angle scattering intensity of liquid water.^{34,48}

The laboratory SAXS apparatus was equipped with a Kratky camera, SAXSess (Anton Paar, Graz, Austria), under 40 kV tube voltage and 50 mA tube current. The line collimated X-rays of Cu K α radiation (1.542 Å in wavelength) were used as the probe. An imaging plate (IP) (FUJIFILM, 100 $\mu\text{m} \times 100 \mu\text{m}$ per pixel) was used for the scattering detector. The distance from the sample to the detector was set at 264.5 mm. The sample solutions were set in a quartz capillary with an inner diameter of 0.98 mm. The X-ray path was evacuated to minimize parasitic scattering from the air. The temperature of the sample was controlled at 25.0 ± 0.1 °C. The exposure time was set at 15 min. The IP recording the scattering signals was scanned using an IP reader, Cyclone scanner (PerkinElmer, Inc.), at 3 min after the

end of each exposure. The image data was integrated to create a 1-dimensional profile using ImageJ⁴⁹ (Wayne Rasband at National, Institute of Health, Bethesda, MD) with the macros in Utah SAXS Tools⁵⁰ (developed by David P. Goldenberg at University of Utah, UT). The absorption of the sample solutions was calculated and corrected by the theoretical mass-absorption coefficients;^{51,52} the protocol was detailed in reference 47. The profile was desmeared using Utah SAXS Tools, by which Lake’s method for desmeared the profiles was applied.⁵³

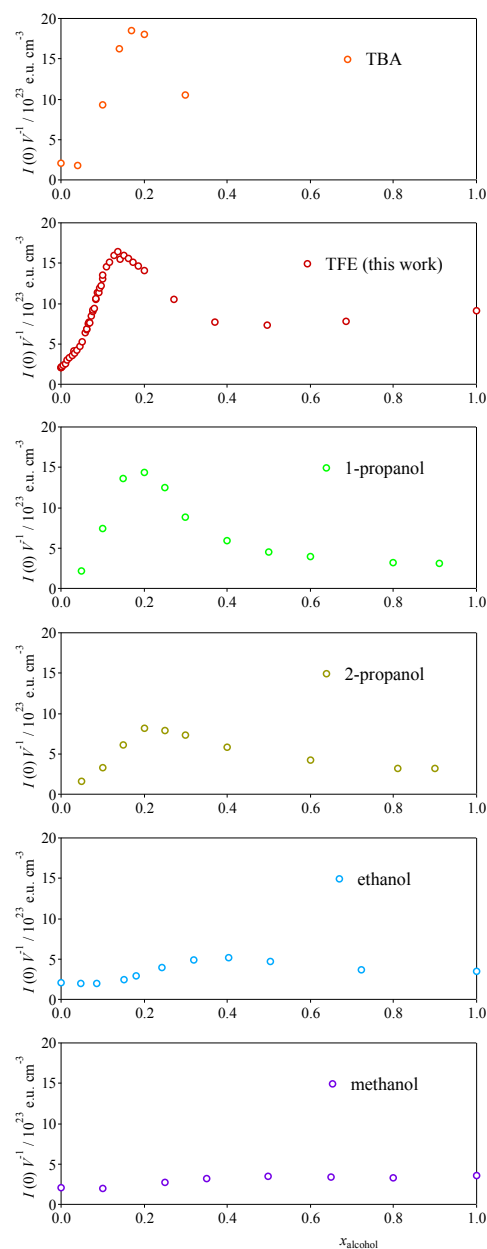


Figure 2. Zero-angle scattering intensity, $I(0)/V$ of TFE–H₂O at 25 °C (this work). For comparison between TFE and other mono-ols studied previously, the concentration dependences of $I(0)/V$ for aqueous solutions of five alcohols are also shown: methanol–H₂O at 25 °C,³⁹ ethanol–H₂O at 20 °C,³⁶ 2-propanol–H₂O at 20 °C,³⁵ 1-propanol–H₂O at 20 °C,³⁵ and TBA–H₂O at 20 °C.³⁴ X_{alcohol} represents the mole fraction of alcohols.

Synchrotron SAXS measurements were performed using the synchrotron radiation at the BL-10C station⁵⁴ of the Photon Factory (PF) at the High Energy Accelerator Research Organization (KEK), Tsukuba. Point collimated X-rays were focused and monochromated using a bent mirror and a bent monochromator. The wavelength of X-rays was set at 1.488 Å. The SAXS signals were acquired using a two-dimensional semiconductor-type detector, PILATUS 300KW or 2M, (DECTRIS Ltd.). The intensity of the incident and transmitted X-rays was monitored using an ionization chamber placed before and after the sample holder. The distance from the sample to the detector was dually set at 1050 or 2010 mm, which was determined using the diffraction pattern of silver behenate, AgBh, for checking the traceability of the data. The sample solutions were set in a standard cell at the beamline station with quartz windows. The sample temperature was controlled at $25.0 \pm 0.1^\circ\text{C}$. The exposure time was set at 1, 2, 4, or 15 min, depending on the scattering intensity of the sample solutions with various concentrations.

2.2 Density and Partial Molar Volume.

The density of the mixture, ρ_m (in unit of g cm^{-3}), was determined by DMA4500 density/specific gravity/concentration meter (Anton Paar), with an oscillating U-tube. The calibration was performed using the density of air and water every day before the measurements. The temperature was kept at $25.00 \pm 0.03^\circ\text{C}$. The uncertainty in density is estimated as $\pm 0.00005 \text{ g cm}^{-3}$ according to the specification of the instrument. Partial molar volumes of TFE, v_{TFE} , and water, v_w , in the mixtures were evaluated from the derivatives of the determined molar volume. The values of v_{TFE} and v_w were used for calculation of the particle fluctuation parameters according to the Bhatia-Thornton theory.²⁸ All the data including the SAXS and the densities are available in references 47 and 55.

3. Results and discussion

3.1 Fluctuation parameters.

3.1.1 Zero-angle scattering intensity

Figures 1 (a-1), (b-1), and (c-1) show scattering profiles in the absolute scale of TFE–H₂O mixtures for $x_{\text{TFE}} = 0.09994$, 0.1372, and 0.1857, around which sharp increases of the SAXS profiles were observed as s decreases. The intense SAXS qualitatively shows the large structural fluctuation of the molecular distribution of the mixtures. Extrapolation to zero-angle of the SAXS profiles was performed to obtain the zero-angle scattering intensity, $I(0)$, using the Lorentz-type function, considering the inhomogeneous structure in molecular distribution and corresponding to large forward scattering. Therefore, we applied the Ornstein-Zernike equation to analyze the present data. The Ornstein-Zernike equation is represented as follows:⁵⁶

$$I(s) = \frac{I(0)}{1 + \xi^2 s^2}, \quad (1)$$

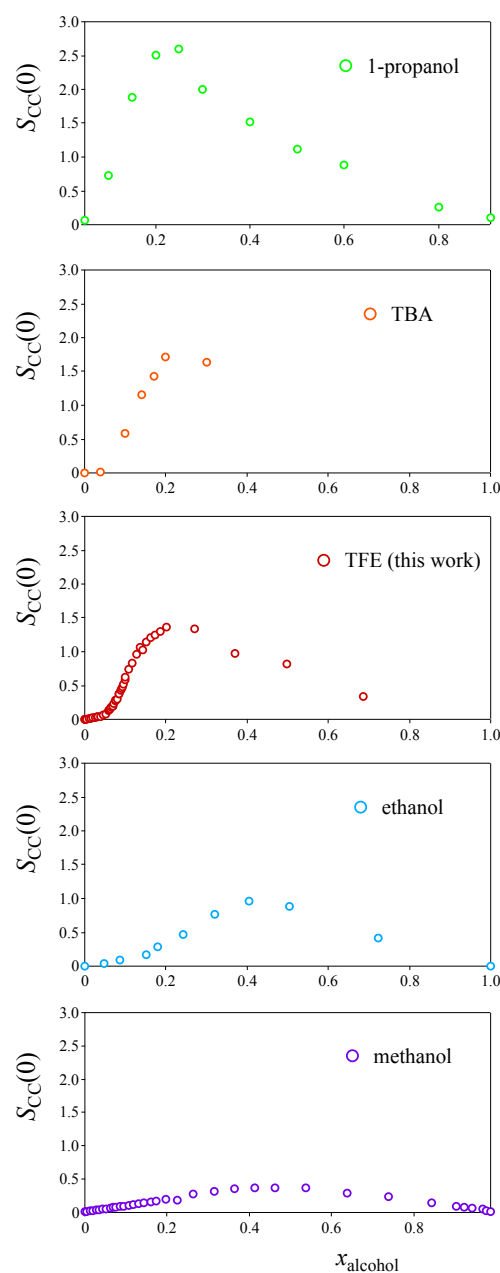


Figure 3. Concentration dependences of the concentration fluctuations for TFE–H₂O mixtures at 25 °C. The fluctuation parameter for aqueous solutions of mono-ols is also shown for methanol–H₂O at 25 °C (obtained with vapor pressure measurement),³⁸ ethanol–H₂O at 20 °C,³⁶ 1-propanol–H₂O at 20 °C,³⁵ and TBA–H₂O at 20 °C.³⁴ Horizontal axis, x_{alcohol} , represents the mole fraction of alcohols. For methanol, $S_{\text{cc}}(0)$ obtained by vapor pressure measurement were shown due to the extremely small fluctuation, namely derivative of chemical potential obtained by vapor pressure measurements, which takes great advantage compared to the SAXS method.⁵⁷ x_{alcohol} represents the mole fraction of alcohols.

where ξ is the Ornstein-Zernike correlation length and s is the scattering parameter defined as $4\pi s \sin \vartheta / \lambda$ (2ϑ : scattering angle, λ : the wavelength of the X-rays). Eq.(1) can be rewritten as:

$$\frac{1}{I(s)} = \frac{1}{I(0)} + \frac{\xi^2}{I(0)} s^2. \quad (2)$$

Eq.(2), the Ornstein-Zernike plot, was applied to examine the extrapolation by fitting procedure. The s range for the fitting is $0.03 < s < 0.2 \text{ \AA}^{-1}$ for $x_{\text{TFE}} = 0.09994$ and 0.1372 , and $0.04 < s < 0.2 \text{ \AA}^{-1}$ for $x_{\text{TFE}} = 0.1857$. The validity of the extrapolation was confirmed in reference 47. As represented by Eq.(2), the plot of $I(s)^{-1}$ against s^2 gives $I(0)$. Figures 1 (a-2), (b-2), and (c-2) show the Ornstein-Zernike plot for the same samples as indicated in Figures 1 (a-1), (b-1), and (c-1) in the absolute scale.

$I(0)$ in units of cm^{-1} was converted into $I(0)/V$ in e.u. cm^{-3} , according to $I(0)/V = I(0)/b_e^2$, where b_e is the electron scattering length ($2.81794 \times 10^{-13} \text{ cm}$); e.u. indicates electron unit. Figure 2 shows the $I(0)/V$ at 25°C against a mole fraction of TFE, x_{TFE} . The $I(0)/V$ values are listed in reference 47. The concentration dependence gives the maximum around at $x_{\text{TFE}} = 0.14$ (40%(v/v)). These results for the maxima were consistent with the previous SAXS analyses with the use of the averaged intensities at $s = 0.1\text{--}0.3 \text{ \AA}^{-1}$ in the literature.¹ The $I(0)/V$ values for aqueous solutions of mono-ols studied previously^{34-36,39} are also shown in Figure 2. The SAXS measurements for aqueous solutions of ethanol, 1-propanol (1P), 2-propanol, and tert-butanol (TBA) were performed at 20°C .³⁴⁻³⁶ To take into account the difference in the temperature, we have measured the SAXS of the TFE aqueous solutions with $x_{\text{TFE}} = 0.20$ at 25.0 and 20.0°C in the same experimental condition. The $I(0)/V$ measured at 25.0°C was $12.81 \times 10^{23} \text{ e.u. cm}^{-3}$ compatible with $13.35 \times 10^{23} \text{ e.u. cm}^{-3}$ at 20.0°C . The difference was estimated to be $0.54 \times 10^{23} \text{ e.u. cm}^{-3}$, which is 4.2% of $12.81 \times 10^{23} \text{ e.u. cm}^{-3}$. As mentioned in the literature,¹ SAXS intensity of TFE is much higher than that of ethanol and slightly higher than that of 1-propanol. As shown in Figure 2, it was clearly observed that the hydrophobicity of alcohol molecules shifts the alcohol concentrations taking the maximum of $I(0)/V$ toward the dilute concentration region. This tendency has also been reported in the data of concentration fluctuation.³⁶ We note that, by 1-propanol (1P)-probing methodology, TFE is more hydrophobic than 1P and is hydrophobic nearly similar to TBA.^{55,57} The 1P-probing methodology determines the hydrophobicity of a solute in its aqueous solutions in dilute region, defined as Mixing Scheme I, where the solute does not form aggregation structure with each other and parameters such as the hydration number of water molecules around the solute are evaluated.⁵⁷ On the other hand, in the previous SAXS study, the hydrophobicity is characterized as the low-concentration shift of the maximum of $I(0)/V$. As discussed later, the $I(0)/V$ in the SAXS method includes the difference and the contrast in electron density of the system and thus more detailed investigations, i.e., concentration fluctuation and Kirkwood and Buff integrals (KBIs), are required (see below).

3.1.2 Particle number fluctuations.

We determined the concentration fluctuation, $S_{\text{CC}}(0) = \bar{N} \langle (\Delta x_{\text{alcohol}})^2 \rangle$, density fluctuation, $S_{\text{NN}}(0) = \langle (\Delta N)^2 \rangle / \bar{N}$, and their cross term, $S_{\text{NC}}(0) = \langle (\Delta N) (\Delta x_{\text{alcohol}}) \rangle$, where \bar{N} , ΔN , and $\Delta x_{\text{alcohol}}$ are the mean value of the number of particles, local deviation from the mean value of the number of particles and that of mole fraction of alcohol, respectively, by combining $I(0)/V$, ρ_m , v_{TFE} , v_{W} , and isothermal compressibility, κ_T . $\langle \rangle$ indicates averaging. The procedure was carried out using the structure factors, $S_{\text{CC}}(s)$, $S_{\text{NN}}(s)$, and $S_{\text{NC}}(s)$, on the basis of the Bhatia and Thornton theory:²⁸

$$I(s) = \bar{N} I_e [\Delta f^2 S_{\text{CC}}(s) + \bar{f}^2 S_{\text{NN}}(s) + 2\bar{f} \Delta f S_{\text{NC}}(s)], \quad (3)$$

where f is the atomic scattering factor in the case of X-ray scattering. The expression Δ of Δf and \bar{f} indicate the difference in f between the components and the mean value of f in the system, respectively. For the X-ray scattering in $s \rightarrow 0$,^{28,58} f is approximated to be Z , the total number of electrons:

$$I(0) = \bar{N} I_e [\Delta Z^2 S_{\text{CC}}(0) + \bar{Z}^2 S_{\text{NN}}(0) + 2\bar{Z} \Delta Z S_{\text{NC}}(0)], \quad (4)$$

where Z is the number of electrons in a particle. According to the Bhatia-Thornton theory, the particle number fluctuations for $s \rightarrow 0$ are evaluated using the zero-angle X-ray scattering intensities together with the thermodynamic quantities of v_i and κ_T as:^{28,58}

$$I(0)/\bar{N} = (x_i Z_i + x_j Z_j)^2 \frac{\bar{N}}{V} k_B T \kappa_T + \left\{ (x_i Z_i + x_j Z_j) \cdot (v_i - v_j) \frac{\bar{N}}{V} - (Z_i - Z_j) \right\}^2 S_{\text{CC}}(0), \quad (5)$$

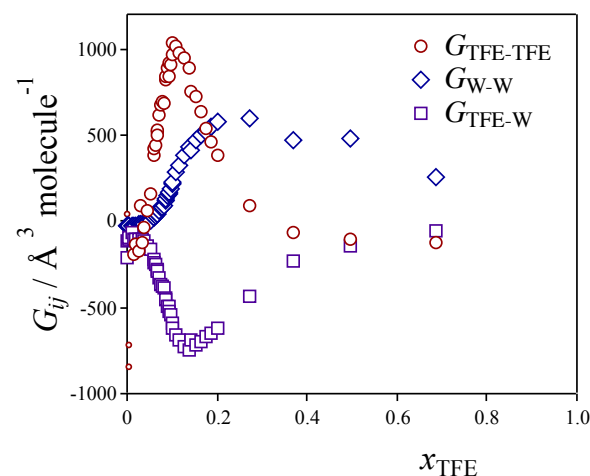


Figure 4. Concentration dependences of the Kirkwood-Buff integrals, $G_{\text{TFE-TFE}}$ (circle), $G_{\text{W-W}}$ (diamond), and $G_{\text{TFE-W}}$ (square), in TFE-H₂O mixture at 25°C .

where x is the concentration in mole fraction and the subscripts i and j indicate component i and j , respectively. The values of SAXS intensities and thermodynamic quantities are listed in reference 47. The values of κ_T for TFE–H₂O mixtures have been reported by Matsuo *et al.*⁵⁹ The values of these quantities at the same concentrations as those for the SAXS measurements were obtained by interpolation. Figure 3 shows the determined concentration fluctuations for TFE–H₂O mixtures. The values of the fluctuation parameters are tabulated in reference 47.

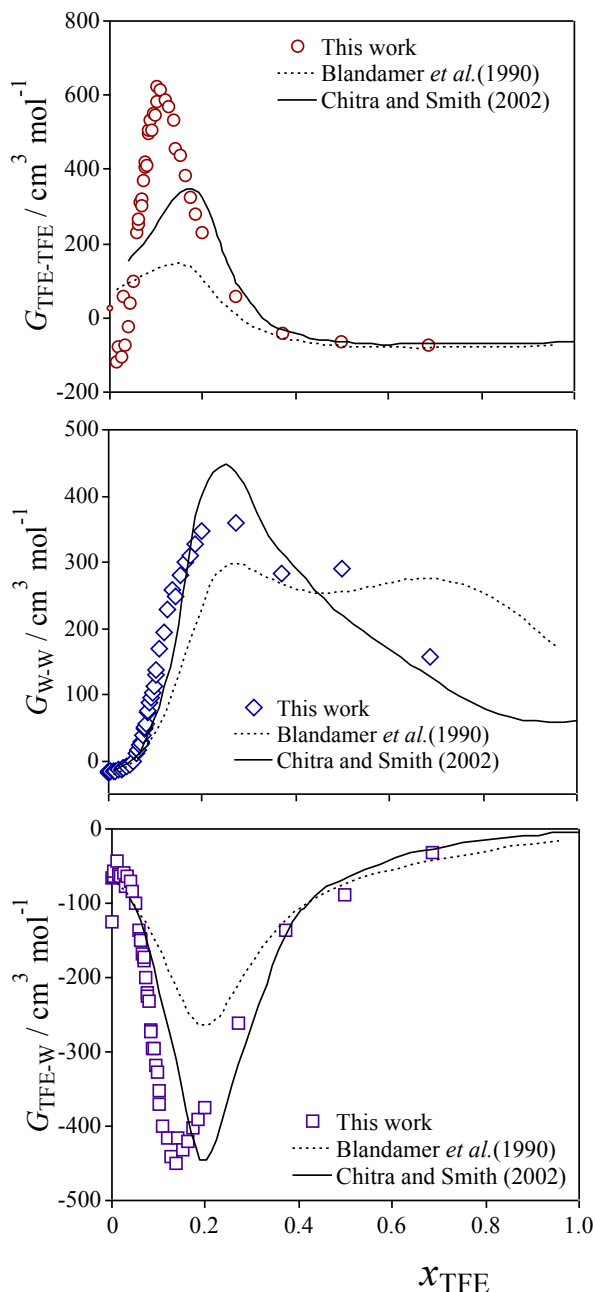


Figure 5. Comparison of the Kirkwood-Buff integrals in TFE–H₂O mixture with the values reported in the literature. Dashed curves show the data reported by Blandamer *et al.* at 25 °C.⁶⁰ Solid curves without marker indicate the data reported by Chitra and Smith at 27 °C.⁶¹

We compared each of the three fluctuations for TFE to those for other mono-ols studied previously.^{34–36,39} It is interesting that the fluctuations of TFE are smaller than those of 1P, though $I(0)/V$ of TFE is larger than the value for 1P, as shown in Figure 2. It was previously suggested that TFE formed the large cluster in TFE–H₂O.^{1,11} However, the large SAXS intensity from TFE–H₂O is caused not only by the aggregation of TFE molecules but also by the higher electron density of TFE molecule. Comparing $I(0)/V$ with the fluctuation parameters for TFE and other mono-ols indicates that only the SAXS intensity does not give the decisive information on the inhomogeneity in molecular distribution of the mixtures. Our analysis of the fluctuation parameters, instead of $I(0)/V$, revealed that the concentration fluctuation ranks as methanol < ethanol << TFE < TBA < 1P: the inhomogeneity of molecular distribution in the TFE aqueous solution is unexpectedly comparable to those of aqueous solutions of the series of mono-ols.

3.1.3 Kirkwood-Buff integrals.

The Kirkwood and Buff integrals (KBIs) is defined as,³¹

$$G_{ij} = \int_0^\infty [g_{ij}(r) - 1] 4\pi r^2 dr, \quad (6)$$

where $g_{ij}(r)$ is the two-body pair distribution function. The meaning of the KBIs is the excess number of distributed particles around one particle in comparison with the mean distribution. For example, G_{ij} means the excess number from the mean value of particles of component j distributed around a particle of component i , including both the inhomogeneity in mixing state and aggregation. The KBIs are calculated from $S_{NN}(0)$, $S_{CC}(0)$ and $S_{NC}(0)$ on the basis of the following equations.³⁰

$$G_{ii} = \frac{V}{N} \left[\frac{1}{x_i^2} \{ x_i^2 S_{NN}(0) + 2x_i S_{NC}(0) + S_{CC}(0) - x_i x_j \} - 1 \right] \quad (7-1)$$

$$G_{jj} = \frac{V}{N} \left[\frac{1}{x_j^2} \{ x_j^2 S_{NN}(0) + 2x_j S_{NC}(0) + S_{CC}(0) - x_i x_j \} - 1 \right] \quad (7-2)$$

$$G_{ij} = \frac{V}{N} \left[\frac{1}{x_i x_j} \{ x_i x_j S_{NN}(0) + (x_j - x_i) S_{NC}(0) + S_{CC}(0) \} \right]. \quad (7-3)$$

The KBIs of $G_{\text{TFE-TFE}}$, $G_{\text{TFE-W}}$, and $G_{\text{W-W}}$ were calculated from the determined particle number fluctuations, where the subscripts of W and TFE represent the component of water and TFE, respectively. Figure 4 shows the concentration dependences of $G_{\text{TFE-TFE}}$, $G_{\text{TFE-W}}$, and $G_{\text{W-W}}$. The values of KBIs are listed in reference 47. $G_{\text{TFE-TFE}}$ was found to have a sharp peak at $x_{\text{TFE}} \sim 0.1$, showing that inhomogeneity of TFE around a TFE molecule is radically enhanced at $x_{\text{TFE}} \sim 0.1$. The large inhomogeneity in molecular distribution is interpreted as the result of the interaction between the respective molecules. $G_{\text{W-W}}$ was evaluated to be also positive, indicating that H₂O molecules

likely interact with H₂O than TFE molecules. The negative $G_{\text{TFE-W}}$ value means that a lesser amount of H₂O molecules are found around a TFE molecule than in random distribution. The concentration dependence shows that $G_{\text{W-W}}$ is enhanced in the higher concentration region than the region in which $G_{\text{TFE-TFE}}$ is enhanced.

Figure 5 shows a comparison of $G_{\text{TFE-TFE}}$, $G_{\text{W-W}}$, and $G_{\text{TFE-W}}$ with literature values,^{60,61} which were obtained using thermodynamic calculations including vapor pressure, combined with fitting functions. For $G_{\text{TFE-TFE}}$, the present result does not show good agreement with the literature values ranging $0 < x_{\text{TFE}} < 0.3$, especially around at $x_{\text{TFE}} = 0.14$ taking the maximum of $G_{\text{TFE-TFE}}$, while these values show excellent agreement with each other in the concentrated region above $x_{\text{TFE}} = 0.4$. We think that the deviation could be caused by difference in evaluation procedure, namely thermodynamic calculation combined with fitting functions vs. the scattering method (direct analysis). We understand that the former takes advantage in the region of small structural fluctuation of the solutions. The latter directly provides KBIs on the basis of the fluctuation parameters, as represented by Eq. (7). As mentioned above, the evaluation of fluctuation parameters for the aqueous solution of methanol by thermodynamic calculation was much better than that by scattering method, as discussed in the caption of Figure 3. The departure becomes more significant in the state having large fluctuations. Therefore, in the concentration range of $0 < x_{\text{TFE}} < 0.3$, we think that $G_{\text{TFE-TFE}}$ by the present SAXS method was superior to the literature values. For $G_{\text{W-W}}$ and $G_{\text{TFE-W}}$, the present results are basically consistent with the literature values by Blandamer *et al.*⁶⁰ and Chitra and Smith.⁶¹ They have utilized thermodynamic methods, which require differentiation to obtain the second derivative quantity of Gibbs energy. We suggest that this could result in an analytical error, especially in a region showing strong concentration dependence of Gibbs energy change.⁵⁷ In the method using small-angle scattering, on the other hand, error becomes smaller as scattering intensity becomes larger, hence the more accurate results will be available in the concentration range with the larger structural fluctuations. The present study for the first time determined the KBIs for TFE–H₂O by the scattering method. We also point out that the scattering method will include relatively larger uncertainty in evaluation of KBIs of the samples in the concentration region with lesser SAXS intensity. Therefore, thermodynamic methods will be better under such situations.⁵⁷

3.1.4 Density fluctuation for each component.

Density fluctuation for each component in the mixture is given by $\rho_i G_{ij}$ for $i = j$ as:³²

$$\frac{\langle(\Delta N_i)^2\rangle}{\bar{N}_i} = \rho_i G_{ii} + 1 \quad (8-1)$$

$$\frac{\langle(\Delta N_j)^2\rangle}{\bar{N}_j} = \rho_j G_{jj} + 1 \quad (8-2)$$

and for $i \neq j$ the same quantities can be written as,

$$\frac{\langle(\Delta N_i)(\Delta N_j)\rangle}{\bar{N}_i} = \rho_j G_{ij} \quad (9-1)$$

$$\frac{\langle(\Delta N_i)(\Delta N_j)\rangle}{\bar{N}_j} = \rho_i G_{ij} \quad (9-2)$$

where ρ_i and ρ_j are the mean number density of components i and j , respectively. \bar{N}_i and \bar{N}_j are the mean number of particles of components i and j within the concerned volume. ΔN_i and ΔN_j are the local deviations of the number of particles of components i and j from the mean value. Figure 6 shows the density fluctuation for each component in TFE–H₂O mixtures. The values are listed in reference 47. The density fluctuation in TFE shows a maximum at $x_{\text{TFE}} \sim 0.12$ while that of H₂O is at $x_{\text{TFE}} \sim 0.2$. Density fluctuation in H₂O is larger than that of TFE. This is because of the difference in the volume of each molecule (van der Waals volumes are 21 Å³ for H₂O and 66 Å³ for TFE⁶² using MOPAC developed by James Stewart). One TFE molecule pushes out more than one H₂O molecule because the volume of a TFE molecule is larger. Therefore, the fluctuation in TFE molecules propagates to larger density fluctuation in H₂O.

3.2 Relation between the KBIs and the helix induction of melittin.

Here, we delineate the relationship between the structural change in a protein and the fluctuation parameters given above. We chose melittin, which is a peptide in bee venom, was chosen as a model peptide/protein because structural changes of melittin induced by the addition of alcohols were investigated for a series of mono-ols.^{43,44} In addition, the tetramer of melittin is transformed into monomers with a coil conformation in neat water without salts and at the natural pH.⁴⁴ In the presence of TFE, the melittin is stable as a monomer with a helix conformation. Here, we employed G_{AA} , *i.e.*, the KBI of alcohol-alcohol molecules, because it was expected to be the fluctuation parameter well correlated with the structure change

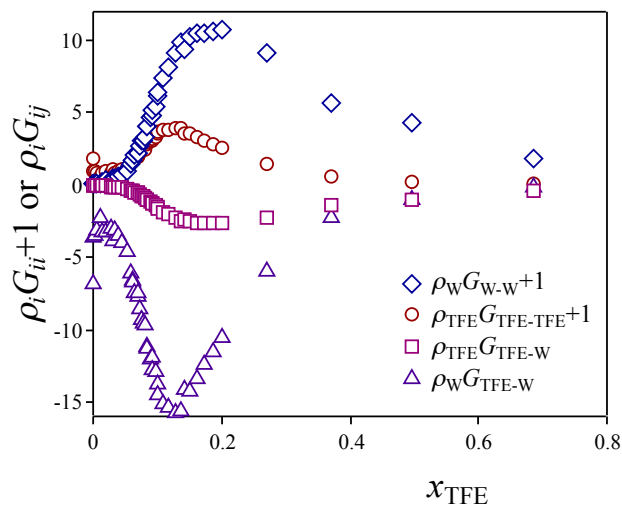


Figure 6. Density fluctuations for each component in TFE–H₂O at 25 °C, $\rho_{\text{TFE}} G_{\text{TFE-TFE}} + 1$ (circle), $\rho_{\text{W}} G_{\text{W-W}} + 1$ (diamond), $\rho_{\text{TFE}} G_{\text{TFE-W}}$ (square), and $\rho_{\text{W}} G_{\text{TFE-W}}$ (triangle).

of proteins and peptides. The investigation of the coil-helix transition of melittin in the presence of TFE will clarify the transition. Although we focus on the discussion based on the coil-helix transition of melittin induced by TFE, the comparison between the structural change in melittin with the parameters is closely related to the general understanding of the structural transition induced by mono-ols.

Figure 7 shows the α -helix contents of melittin in various alcohol aqueous solutions^{43,44} together with G_{AA} .³⁴⁻³⁶ The subscript A represents the given alcohol. On inspection of Figure 7, it is suggested that alcohol with the stronger hydrophobicity range. To see this trend more clearly, the ordinate values at a half of total variations of molar ellipticities at 222 nm, $-[\theta]_{222}$,

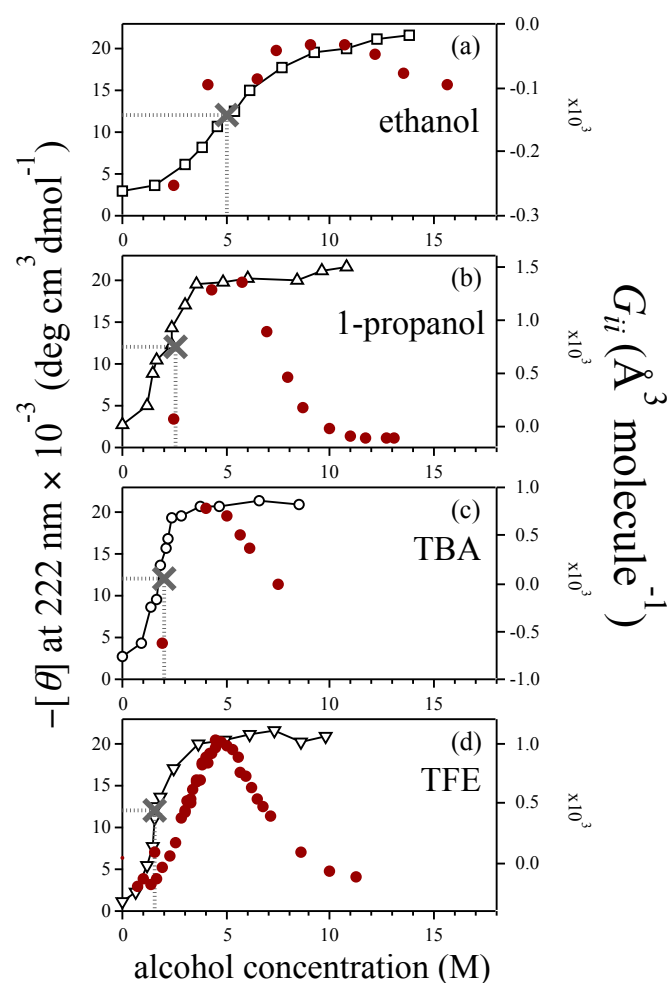


Figure 7. α -Helix contents of melittin in various alcohol aqueous solutions evaluated with CD spectroscopy at 20 °C and the Kirkwood-Buff integral G_{AA} of the alcohol aqueous solutions. These alcohols are (a) ethanol, (b) 1-propanol, (c) *tert*-butanol (TBA), and (d) TFE. The solid lines with marker represent α -helix contents of melittin. The red and solid circles indicate G_{AA} . The gray crosses represent the midpoints of denaturation. The CD data were taken from the literature.^{43,44} The G_{AA} data were taken for ethanol,³⁶ 1-propanol,³⁵ and TBA.³⁴ Concentration in mole fraction was converted into that in molar (M) using volumetric data reported in literature for ethanol,⁷⁰ 1-propanol,⁷⁰ and TBA.⁷¹

seems to induce the helix conformation more sharply and that the induction is observed at the lower alcohol concentration were set as the midpoint of denaturation for each panel, as represented by the gray cross in the figure: the midpoint means 50% in the conversion. The concentrations of alcohol at the midpoints indicate the efficiency of alcohol on the induction of structural change. In terms of this, the ranking would be ethanol < 1P < TBA < TFE. Furthermore, the previous study suggested that cluster formation of alcohols is responsible for the denaturation of biomolecules.¹ However, as shown in Figure 7, the conformational change of melittin was also observed in the concentration region without cluster formation of alcohols.

As shown in Figures 7 b-d, the KBIs of G_{AA} take maxima at the concentrations where structural changes of melittin seem to be almost complete. Therefore, it is suggested that the aggregation of alcohol molecules leads to stabilization of the α -helical structure, which was already induced and formed by addition of alcohols. As shown in Figure 4, the maximum of $G_{TFE-TFE}$ was determined as $x_{TFE} \sim 0.10$ ($\sim 31\%$ (v/v), ~ 4.5 M). The dielectric constant of TFE–H₂O mixtures at this composition was estimated to be 64 from the literature data.¹ As shown in Figure 7d, the α -helix content of melittin in TFE–H₂O mixtures at this concentration is observed as a plateau. On the other hand, α -helix content of melittin in ethanol–H₂O mixtures with the same dielectric constant corresponds to the value around at the midpoint. These results indicate that the stability of an α -helix in TFE–H₂O mixtures under the state that the α -helix content reaches the plateau cannot be explained only by the dielectric constant. Hong et al., invoked enhancement of the TFE–TFE interaction to explain the anomalous capability of TFE in inducing helices. We, therefore, investigated whether the maximum G_{AA} had a relation with the ability to induce helices or not. In terms of the value of individual mole fraction and the magnitude of the maximum G_{AA} , the ranking was reordered as ethanol < TBA < TFE < 1P. Hence, the large values of G_{AA} , which means strong attraction between alcohol molecules with each other, are not necessarily important to induce α -helix into melittin. This looks unexpectedly inconsistent with the previously proposed mechanism.¹ To address this inconsistency, we further analyzed the data by applying a modern theory by Smith *et al.*^{45,46} (see next).

3.3 Evaluation of difference in preferential binding between the coil and helix

To gain an understanding of the cosolvent-induced coil-helix transition of proteins and peptides, we quantitatively evaluated the difference in preferential binding of TFE to melittin between the coil and helix conformation. The preferential binding to a protein in an aqueous solution represents the property of competition between the interaction of cosolvent molecules to the protein and that of water molecules. In the case of the process of the addition of cosolvent, the preferential binding clarifies the state in exchange of solvation water molecules with cosolvent molecules around protein. As pointed out by Smith *et al.*,^{45,46} the preferential binding is an important concept for understanding the structural changes of proteins and peptides

induced by cosolvent because the effect of cosolvent on the excess chemical potential of biomolecules has been quantified on the basis of the concept of preferential binding of cosolvent to biomolecules.

We describe the procedure for evaluating the difference in preferential binding of cosolvent to biomolecules proposed in the present study. Several models for expression of difference in the preferential binding have been proposed.^{45,63,64} In the present study, the quantity was evaluated on the basis of the preferential binding parameter, Γ_{23} , proposed by Smith *et al.*^{45,46} For the ternary system, *water, protein, and alcohol are defined as component 1, 2, and 3, respectively.* The solution is considered as the infinitely dilute system in protein concentration. The difference in solvation free energy of protein, $\mu_{s,2}$, and that in preferential binding parameter, Γ_{23} , between the coil (c) and helix (h) states is defined as:

$$\Delta\mu_{s,2} \equiv \mu_{s,2}^h - \mu_{s,2}^c, \quad (10)$$

$$\Delta\Gamma_{23} \equiv \Gamma_{23}^h - \Gamma_{23}^c. \quad (11)$$

Hereafter, the superscripts c and h in all thermodynamic quantities denote the coil and the helix states, respectively. In the present study, we define the Gibbs energy of the coil-helix transition, ΔG , using two factors: the intra-molecular interaction free energy of the protein in a vacuum, E_{intra} , and the solvation free energy of protein in aqueous solution, $\mu_{s,2}$, as follows:^{65,66}

$$\begin{aligned} \Delta G &= \bar{\mu}_h - \bar{\mu}_c \\ &= (E_{\text{intra}}^h + \mu_{s,2}^h) - (E_{\text{intra}}^c + \mu_{s,2}^c) = \Delta E_{\text{intra}} + \Delta\mu_{s,2}. \end{aligned} \quad (12)$$

$\bar{\mu}_h$ and $\bar{\mu}_c$ in Eq. (12) are the standard chemical potentials of the helix and the coil, respectively. Smith *et al.* have defined the parameters of Γ_{23} for the helix and a_{33} using the KBIs and the number density of component i , ρ_i , as:⁴⁶

$$\Gamma_{23}^h \equiv \rho_3(G_{23}^h - G_{21}^h), \quad (13)$$

$$a_{33} \equiv \frac{1}{1 + \rho_3(G_{33} - G_{31})}. \quad (14)$$

On the basis of the definition of Eqs. (13) and (14), $\bar{\mu}_h$ for the helix is expressed by the following equation:⁴⁶

$$\beta \left(\frac{\partial \bar{\mu}_h}{\partial \ln \rho_3} \right)_{T,P} = - \frac{\rho_3(G_{23}^h - G_{21}^h)}{1 + \rho_3(G_{33} - G_{31})} \equiv -\Gamma_{23}^h a_{33}, \quad (15)$$

where $\beta = 1/RT$ (R is the gas constant and T is temperature). This equation provides crucial insights into cosolvent effects arising from the preferential binding of cosolvent to the helix: $\bar{\mu}_h$ decreases with an increase in the cosolvent density ρ_3 , resulting

in stabilization of the helix if the cosolvent preferentially binds to the helix, namely, $\Gamma_{23}^h > 0$, under a typical condition $a_{33} > 0$. We can attribute the cosolvent-concentration dependence of $\bar{\mu}_h$ to both the effects of the preferential binding (Γ_{23}^h) and aggregation of cosolvent (a_{33}). Eq. (15) can be rewritten for the coil state in the same manner as the helix state. Using these equations together with Eq. (12), the difference in the preferential binding, $\Delta\Gamma_{23} \equiv \Gamma_{23}^h - \Gamma_{23}^c$, is represented as:

$$\Delta\Gamma_{23} = - \frac{\beta}{a_{33}} \left(\frac{\partial \Delta G}{\partial \ln \rho_3} \right)_{T,P} = - \frac{\beta \rho_3}{a_{33}} \left(\frac{\partial \Delta G}{\partial \rho_3} \right)_{T,P}. \quad (16)$$

As Eq. (14) defines, a_{33} is evaluated using the number density of TFE, ρ_3 , and the KBIs between the solvent components of water and alcohol, i.e., G_{W-W} and $G_{\text{TFE-W}}$, in the pure TFE–H₂O solution. On the right-hand side of Eq. (16), we simply applied ΔG obtained from the TFE concentration dependence of the helix content, as described below. Equation (12) gives the partial differentiation,

$$\begin{aligned} &\left(\frac{\partial \Delta G}{\partial \rho_3} \right)_{T,P}, \text{ as,} \\ &\left(\frac{\partial \Delta G}{\partial \rho_3} \right)_{T,P} = \left(\frac{\partial \Delta E_{\text{intra}}}{\partial \rho_3} \right)_{T,P} + \left(\frac{\partial \Delta \mu_{s,2}}{\partial \rho_3} \right)_{T,P}. \end{aligned} \quad (17)$$

ΔE_{intra} is independent of solvent species and their concentration because ΔE_{intra} involves the intramolecular interaction free energies for free molecules in a vacuum as mentioned above. Therefore, ΔE_{intra} takes a constant value and hence the first term in the right-hand side of Eq. (17),

$$\left(\frac{\partial \Delta E_{\text{intra}}}{\partial \rho_3} \right)_{T,P},$$

is equal to zero. Thereby, we found a useful equation,

$$\left(\frac{\partial \Delta G}{\partial \rho_3} \right)_{T,P} = \left(\frac{\partial \Delta \mu_{s,2}}{\partial \rho_3} \right)_{T,P}, \quad (18)$$

indicating that the cosolvent-concentration dependence of ΔG is attributable to that of the solvation free energy difference. ΔG is experimentally accessible applying helix content, f_h , according to the following relationships (see Supporting Information):

$$\Delta G = -RT \ln \frac{f_h}{1-f_h}. \quad (19)$$

The helix content was determined from the mean residue ellipticity at 222 nm, $[\theta]_{222}$,^{43,44} on the basis of the assumption of a two-state model in the coil-helix transition: note that the helix-coil transition theory such as Zimm-Bragg theory⁶⁷ could be an option to determine ΔG .

Literature^{43,44} gave f_h for melittin in the wide concentration range of alcohols. Empirically, ΔG has been established as a simple function of alcohol concentration, $[Alcohol]$, (in units of mol/L, M) as follows.

$$\Delta G = \Delta G_0 - m[Alcohol], \quad (20)$$

where ΔG_0 is ΔG at $[Alcohol] = 0$ and m indicates the slope, i.e., the dependence of ΔG on $[Alcohol]$. We confirmed that some variation of m -value does not affect the detailed discussion of TFE concentration dependence of the determined $\Delta \Gamma_{23}$.

3.4 Two different regimes in the excess preferential binding mechanism of alcohol to protein

We quantitatively evaluated the difference in preferential binding of cosolvent to melittin monomer between the coil and helix state, $\Delta \Gamma_{23}$, on the basis of the calculation procedure proposed above. Figure 8 shows the evaluated $\Delta \Gamma_{23}$ together with a_{33} parameter as a function of TFE molarity ([TFE]). For comparison, $\Delta \Gamma_{23}$ obtained by assuming $a_{33} = 1$, namely, obtained from an ideal homogeneous model for a_{33} , is also shown. $a_{33} = 1$ means a homogenous molecular distribution of water and TFE, where G_{33} is always equal to G_{31} , whereas G_{33} and G_{31} are not necessarily equal to zero. In such an ideal homogeneous model for alcohol–water mixture, solvent-mediated interactions, at least, do not play a crucial role in the excess preferential binding of alcohol to the helix. At the concentrations lower than ~ 2 M ($x_{TFE} < \sim 0.04$), the value of $\Delta \Gamma_{23}$ is comparable with $\Delta \Gamma_{23}$ for $a_{33} = 1$, indicating that the excess preferential binding of TFE to the helix is predominantly caused by the direct interaction between the helix and TFE, and has the ability to achieve the helix content larger than the midpoint of denaturation (Figure 7d). These findings demonstrate that the concentration of TFE at the midpoint being lower than that of the other alcohol molecules, i.e., the higher ability of helix induction by TFE is attributed to the stronger direct interactions between the helix and TFE, namely, both the dipole-dipole interactions and London dispersion forces, which should originate from the chemical nature of CF_3 – in TFE molecule.⁶⁸

On the other hand, at the concentrations higher than ~ 2 M ($x_{TFE} > \sim 0.04$), $\Delta \Gamma_{23}$ is always larger than $\Delta \Gamma_{23}$ for $a_{33} = 1$, indicating that, in addition to the effect of the direct interaction between the helix and TFE, the excess preferential binding of TFE is enhanced by structural fluctuation effects of TFE–H₂O mixture. In fact, the concentration dependence of $\Delta \Gamma_{23}$ is well correlated with that of a_{33} which should contain all the effects of structural fluctuation of TFE–H₂O mixture on the excess preferential binding of TFE. As shown in Figure 8, $\Delta \Gamma_{23}$ attained the maximum value at $x_{TFE} = \sim 0.2$, which was close to the maximum of the concentration fluctuation ($x_{TFE} = \sim 0.2$ (~ 7.1 M), see Figure 3) and $G_{TFE-TFE}$ ($x_{TFE} = \sim 0.1$ (~ 4.4 M), see Figure 4). These observations suggest that the excess preferential binding of TFE is enhanced by the large structural fluctuation of TFE–H₂O solvent due to the aggregation of TFE molecules. The

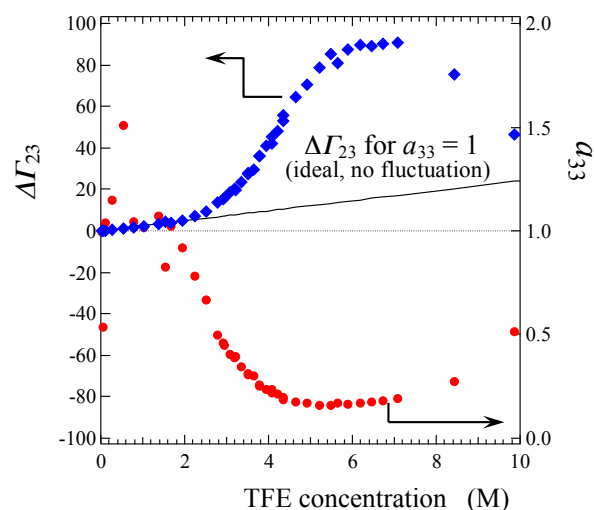


Figure 8. Difference in the preferential binding of TFE molecule to melittin between the coil and helix conformation estimated by the preferential binding parameter proposed by Smith *et al.*^{45,46} The a_{33} parameter calculated by KBIs is also shown. We employed 6.0 as the m -value for melittin⁴³ in Eq. 20. For comparison, $\Delta \Gamma_{23}$ obtained by assuming $a_{33} = 1$, namely, obtained from an ideal homogeneous model for a_{33} , is also shown as a solid line. The values in this figure and unit conversion from x_{TFE} to [TFE] (M) are given in Supporting Information.

concentration at the maximum of $\Delta \Gamma_{23}$ shown in Figure 8 corresponds to the concentration region for saturation of the helix induction by TFE, as shown in Figure 7.

As shown in Figure 4, $G_{TFE-TFE}$ has negative values or values around zero in the dilute region ($x_{TFE} < \sim 0.04$), suggesting that aggregation between TFE molecules does not occur or is not experimentally detected in this region. This behavior corresponds to the concept of the Mixing Scheme I, proposed by Koga; a non-aggregation region between solutes in aqueous solutions identified in the dilute region.⁵⁷ In fact, our previous calorimetric analysis found that the Mixing Scheme I of TFE–H₂O is at $x_{TFE} < 0.04$.⁵⁵ Correspondingly, as shown in Figure 8, a_{33} likely took the value larger than 1 at the TFE mole fractions $< \sim 0.03$ ($< \sim 1.5$ M), implying that there was a possibility so that $\Delta \Gamma_{23}$ became lower than $\Delta \Gamma_{23}$ obtained from the ideal homogeneous model of a_{33} ($a_{33} = 1$). It can be said that the precise KBIs data obtained from the scattering method enable us to observe the specific and complex behavior. The details should be clarified by experiments focusing on the dilute region, Mixing Scheme I.

3.5 Gibbs energy of coil-helix transition

To better understand the coil-helix transition of protein by addition of alcohol, we discuss alcohol-concentration dependence of the Gibbs energy of the coil-helix transition both in intramolecular interaction free energy of protein, the intramolecular interaction free energy of protein in a vacuum, and the solvation free energy of the protein based on the difference in the preferential binding of TFE. Figure 9 represents

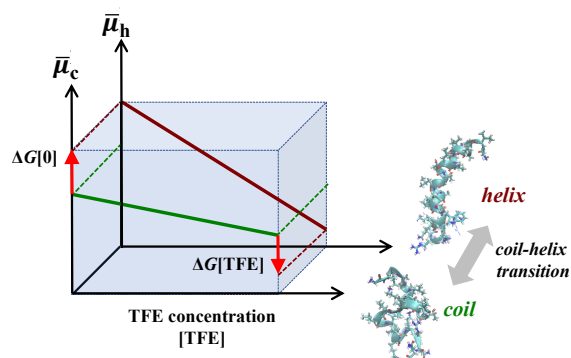


Figure 9. Schematic representation of ΔG vs. TFE concentration for the coil-helix transition or the stability of helix conformation. $\Delta G[0]$ expresses ΔG under the condition in neat water.

the schematic of Gibbs energy of the coil-helix transition of melittin. As mentioned above (Eq.(12)), ΔG depends on E_{intra} and $\mu_{s,2}$, and E_{intra} is independent of the concentration of [TFE]. Thus the larger decrease of $\bar{\mu}_h$ compared to $\bar{\mu}_c$ with increasing [TFE] is attributed to the larger decrease of $\mu_{s,2}^h$ than $\mu_{s,2}^c$. If $\mu_{s,2}^h$ is more largely decreased upon adding TFE, the helix should preferentially bind TFE than water. This observation is interpreted by the stronger interactions with the part of CF_3CH_2 - in TFE than water due to both the dipole-dipole interactions and London dispersion forces between the helix and TFE. In addition, since the OH in TFE interacts with water forming hydrogen bonds, micelle-like structures by TFE would be formed surrounding the helix. The detailed molecular mechanism for the binding of cosolvent molecules to biomolecules should be clarified using various kinds of approaches in future investigations.

3.6 Relationship between the helix induction and the solution structure

Figure 10 shows the relationship between the helix induction by TFE and the mixing state of the aqueous solution of TFE. Our thermodynamic analysis revealed a relationship among structural fluctuations of TFE–H₂O mixture, the excess preferential binding of TFE to the helix, as well as the conformational change of protein in TFE–H₂O mixture. It turned out that, in the dilute concentration region lower than 2 M of TFE ($x_{\text{TFE}} < \sim 0.04$), TFE with lack of clustering (i.e., aggregation of TFE molecules among themselves) is capable of inducing the helix (Figure 8). On the other hand, solvent fluctuation effects along with aggregation of TFE molecules (indicated as a_{33} in Figure 8) enhance the stabilization of the helix in the higher concentration region above ~ 2 M of TFE ($x_{\text{TFE}} > \sim 0.04$). At ~ 5 M ($x_{\text{TFE}} = \sim 0.12$), where clustering of TFE molecules is the most favorable ($G_{\text{TFE-TFE}}$ takes a maximum), the helix is almost completely induced. The almost saturated helix induction cannot be explained only by the reduction of the dielectric constant (from 80 to ~ 64),¹ because the helix content of melittin in ethanol–H₂O mixture with the same dielectric constant corresponds to the value around at the midpoint (Figure 7). The feature of non-aggregation between TFE molecules characterized by the mixing scheme I^{57,69} is consistent with the

ideal homogeneous model of TFE–H₂O mixture ($a_{33} = 1$), which quantitatively reproduces the excess preferential binding of TFE to the helix.

4. Conclusions

We determined the fluctuation parameters, such as particle number fluctuations: $S_{\text{CC}}(0)$, $S_{\text{NN}}(0)$, and $S_{\text{NC}}(0)$, the KBIs calculated by the particle number fluctuations: $G_{\text{TFE-TFE}}$, $G_{\text{TFE-W}}$, and $G_{\text{W-W}}$, and the density fluctuations of each component for TFE–H₂O mixture using SAXS method. Previously, cluster formation (i.e., aggregation) of TFE in TFE–H₂O mixture was qualitatively evaluated on the basis of an increase of the SAXS intensity.^{1,11} However, it was found that the inhomogeneity and the aggregation aspects of the mixture are not as strong as expected only from SAXS intensities.

In the present study, relationships between the structural fluctuations of TFE–H₂O mixtures, the excess preferential binding of TFE to the helix, as well as the conformational change of protein in TFE–H₂O mixture were investigated. By combining the KBIs and the helix content, we quantitatively evaluated the difference in preferential binding of TFE to protein between the coil and helix conformations, $\Delta\Gamma_{23}$, on the basis of the theory of preferential binding proposed by Smith *et al.*^{45,46} We found two different regimes in the excess preferential binding of TFE to the helix compared to the coil. In the first regime, i.e., dilute TFE concentration region lower than ~ 2 M ($x_{\text{TFE}} < \sim 0.04$), the excess preferential binding of TFE to the helix is caused predominantly by the direct interaction between the helix and TFE. The higher ability of helix induction by TFE than by the other alcohols at the dilute concentrations of alcohol is attributable to the stronger direct interactions between the helix and TFE, i.e., the dipole-

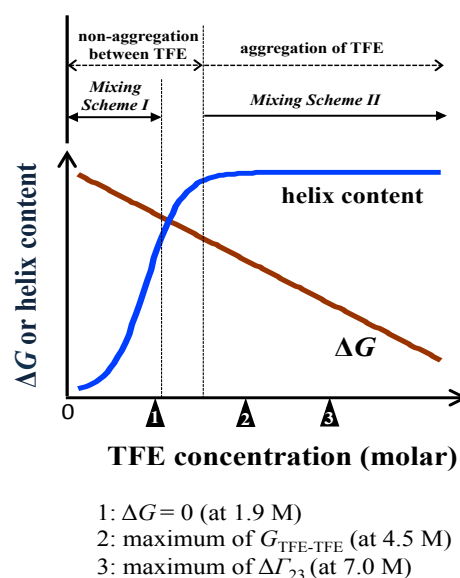


Figure 10. Relationship between the helix induction of melittin by the addition of TFE and the mixing state of the aqueous solution of TFE. The concentration at $\Delta G = 0$ is evaluated on the basis of the two-state model for melittin, which could depend on the model and the protein investigated.

dipole interactions and London dispersion forces, which are linked to the chemical nature of CF_3^- in TFE. In the second regime, i.e., the TFE concentrations higher than 2 M ($x_{\text{TFE}} > 0.04$), in addition to the effects of strong direct interactions between the helix and TFE, significant structural fluctuations of TFE– H_2O mixture enhance the excess preferential binding of TFE to the helix, which results in stronger stabilization of helical conformations. We can confirm that these conclusions do not depend on the m -value in Eq. (20) (see Figure 11), thus indicating that the mechanism presented here on alcohol-induced helix formation is a general cosolvent effects of TFE on peptides and proteins (even if these molecules possess a different m -value).

The effects of structural fluctuations of alcohol–water mixtures on the preferential binding of alcohol molecules to melittin had been phenomenologically pointed out by Hong *et al.* on the basis of the correlation between the ability of helix induction and the aggregation of alcohol molecules in alcohol–water mixtures.¹ On the other hand, in the present study, we quantified the excess preferential binding of TFE to

the helix as $\Delta\Gamma_{23}$, and quantitatively demonstrated the relationship between $\Delta\Gamma_{23}$ and effects of the structural fluctuations of TFE– H_2O mixtures on $\Delta\Gamma_{23}$ which is characterized by a_{33} . The approach presented here to quantify the change in preferential binding of cosolvent molecules to proteins and peptides upon conformation transitions will contribute to reveal the molecular mechanism of the preferential binding as well as to gain the deeper insight into conformational transition induced by cosolvent molecules.

Conflicts of interest

There are no conflicts to declare.

Acknowledgements

We are grateful to PF at KEK for providing the opportunity to perform the SAXS experiments. We express thanks to Prof. Naoto Yonezawa at Chiba University for his helpful discussion about CD data treatment. This work was partially supported by a JSPS grant-in-aid for Scientific Research (KAKENHI Nos. 17073002, 24550009, and 15K05376).

Notes and references

- 1 D.-P. Hong, M. Hoshino, R. Kuboi and Y. Goto, *J. Am. Chem. Soc.*, 1999, **121**, 8427–8433.
- 2 P. Doty, K. Imahori and E. Klemperer, *Proc. Natl. Acad. Sci. U. S. A.*, 1958, **44**, 424–431.
- 3 M. Buck, *Q. Rev. Biophys.*, 1998, **31**, 297–355.
- 4 R. E. Weber and C. Tanford, *J. Am. Chem. Soc.*, 1959, **81**, 3255–3260.
- 5 G. Conio, E. Patrone and S. Brighetti, *J. Biol. Chem.*, 1970, **245**, 3335–3340.
- 6 A. M. Tamburro, A. Scatturin, R. Rocchi, F. Marchiori, G. Borin and E. Scoffone, *FEBS Lett.*, 1968, **1**, 298–300.
- 7 J. E. Brown and W. A. Klee, *Biochemistry*, 1971, **10**, 470–476.
- 8 L. F. Liebes, R. Zand and W. D. Phillips, *Biochim. Biophys. Acta*, 1975, **405**, 27–39.
- 9 J. W. Nelson and N. R. Kallenbach, *Proteins*, 1986, **1**, 211–217.
- 10 A. Jasanoff and A. R. Fersht, *Biochemistry*, 1994, **33**, 2129–2135.
- 11 S. Kuprin, A. Gräslund, A. Ehrenberg and M. H. Koch, *Biochem. Biophys. Res. Commun.*, 1995, **217**, 1151–1156.
- 12 T. Imai, A. Kovalenko, F. Hirata and A. Kidera, *Interdiscip. Sci. Comput. Life Sci.*, 2009, **1**, 156–160.
- 13 E. J. Arthur, J. T. King, K. J. Kubarych and I. Charles L Brooks, *J. Phys. Chem. B*, 2014, **118**, 8118–8127.
- 14 P. Westh and Y. Koga, *J. Phys. Chem. B*, 1997, **101**, 5755–5758.
- 15 Y. Koga, P. Westh, C. Trandum and C. A. Haynes, *Fluid Phase Equilib.*, 1997, **136**, 207–221.
- 16 E. Chatani, H. Yagi, H. Naiki and Y. Goto, *J. Biol. Chem.*, 2012, **287**, 22827–22837.
- 17 C. M. Othon, O. H. Kwon, M. M. Lin and A. H. Zewail, *Proc. Natl. Acad. Sci. U. S. A.*, 2009, **106**, 12593–12598.
- 18 W. Liu, D. Bratko, J. M. Prausnitz and H. W. Blanch, *Biophys. Chem.*, 2004, **107**, 289–298.
- 19 N. Javid, K. Vogtt, C. Krywka, M. Tolan and R. Winter, *Chemphyschem*, 2007, **8**, 679–689.
- 20 M. Dhanasekaran, M. M. Palian, I. Alves, L. Yeomans, C. M. Keyari, P. Davis, E. J. Bilsky, R. D. Egleton, H. Yamamura, N. E.

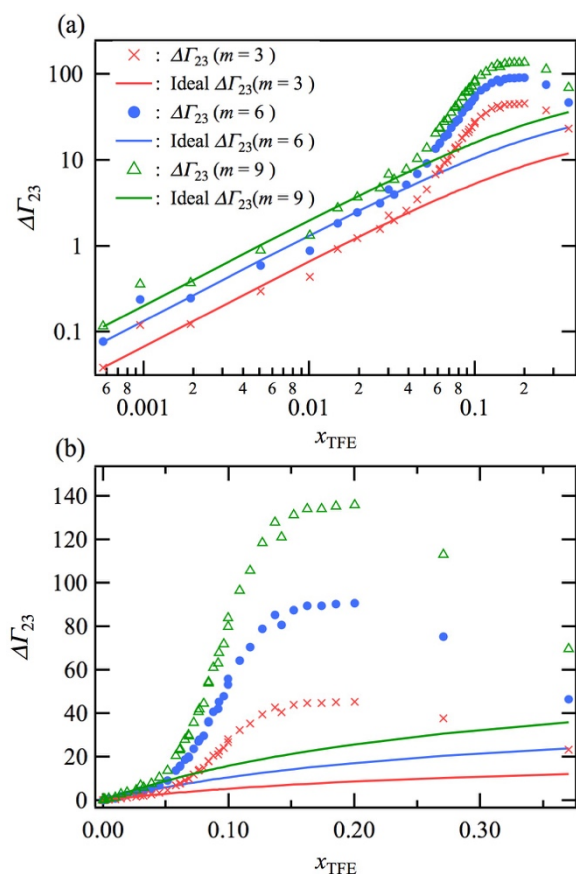


Figure 11. $\Delta\Gamma_{23}$ of TFE to various proteins/peptides between the coil and helix conformation obtained using varying m -value as a function of mole fraction x_{TFE} . For comparison, $\Delta\Gamma_{23}$ obtained by assuming $a_{33} = 1$, namely, obtained from the ideal homogeneous model for a_{33} , is also shown as solid lines. (a) is the logarithmic graph of (b). The results provided by the m -value of 6 are the same as those shown in Figure 8.

- Jacobsen, G. Tollin, V. J. Hruby, A. F. Porreca and R. Polt, *J. Am. Chem. Soc.*, 2005, **127**, 5435–5448.
- 21 K. Yoshida, Y. Fukushima and T. Yamaguchi, *J. Mol. Liq.*, 2014, **189**, 1–8.
- 22 J. T. Gerig, *J. Phys. Chem. B*, 2014, **118**, 1471–1480.
- 23 J. T. Gerig, *J. Phys. Chem. B*, 2016, **120**, 11256–11265.
- 24 D. Mohanta and M. Jana, *Physical Chemistry Chemical Physics*, 2018, **20**, 9886–9896.
- 25 J. T. Gerig, *J. Phys. Chem. B*, 2019, **123**, 3248–3258.
- 26 K. R. Harris, P. J. Newitt and Z. J. Derlacki, *J. Chem. Soc. Faraday Trans.*, 1998, **94**, 1963–1970.
- 27 T. Takamuku, T. Kumai, K. Yoshida, T. Otomo and T. Yamaguchi, *J. Phys. Chem. A*, 2005, **109**, 7667–7676.
- 28 A. B. Bhatia and D. E. Thornton, *Phys. Rev. B*, 1970, **2**, 3004–3012.
- 29 Y. Koga, *Chem. Phys. Lett.*, 1984, **111**, 176–180.
- 30 K. Nishikawa, *Chem. Phys. Lett.*, 1986, **132**, 50–54.
- 31 J. G. Kirkwood and F. P. Buff, *J. Chem. Phys.*, 1951, **19**, 774–777.
- 32 K. Nishikawa, H. Hayashi and T. Iijima, *J. Phys. Chem.*, 1989, **93**, 6559–6565.
- 33 A. Nitta, T. Morita, S. Saita, Y. Kohno, H. Ohno and K. Nishikawa, *Chem. Phys. Lett.*, 2015, **628**, 108–112.
- 34 K. Nishikawa, Y. Kodera and T. Iijima, *J. Phys. Chem.*, 1987, **91**, 3694–3699.
- 35 H. Hayashi, K. Nishikawa and T. Iijima, *J. Phys. Chem.*, 1990, **94**, 8334–8338.
- 36 K. Nishikawa and T. Iijima, *J. Phys. Chem.*, 1993, **97**, 10824–10828.
- 37 K. Nishikawa, Y. Kasahara and T. Ichioka, *J. Phys. Chem. B*, 2002, **106**, 693–700.
- 38 J. Hu, C. A. Haynes, A. H. Wu, C. M. Cheung, M. M. Chen, E. G. Yee, T. Ichioka, K. Nishikawa, P. Westh and Y. Koga, *Can. J. Chem.*, 2003, **81**, 141–149.
- 39 T. Morita and K. Nishikawa, *Chem. Phys. Lett.*, 2004, **389**, 29–33.
- 40 K. Nishikawa and M. Takematsu, *Chem. Phys. Lett.*, 1994, **226**, 359–363.
- 41 K. Nishikawa and T. Morita, *J. Phys. Chem. B*, 1997, **101**, 1413–1418.
- 42 T. Morita, H. Miyagi, Y. Shimokawa, H. Matsuo and K. Nishikawa, *Jpn. J. Appl. Phys.*, 1998, **37**, L768–L770.
- 43 N. Hirota, Y. Goto and K. Mizuno, *Protein Sci.*, 1997, **6**, 416–421.
- 44 N. Hirota, K. Mizuno and Y. Goto, *J. Mol. Biol.*, 1998, **275**, 365–378.
- 45 P. E. Smith, *Biophys. J.*, 2006, **91**, 849–856.
- 46 V. Pierce, M. Kang, M. Aburi, S. Weerasinghe and P. E. Smith, *Cell Biochem. Biophys.*, 2008, **50**, 1–22.
- 47 Ohgi, H. Master's thesis, Chiba university 2016.
- 48 M. Morimoto, H. Imamura, S. Shibuta, T. Morita, K. Nishikawa, H. Yamamoto, R. Tanaka and T. Takanohashi, *Energy Fuels*, 2015, **29**, 5737–5743.
- 49 C. A. Schneider, W. S. Rasband and K. W. Eliceiri, *Nat. Methods*, 2012, **9**, 671–675.
- 50 D. P. Goldenberg and B. Argyle, *Biophys. J.*, 2014, **106**, 895–904.
- 51 E. B. Saloman, J. H. Hubbell and J. H. Scofield, *Atomic Data and Nuclear Data Tables*, 1988, **38**, 1–196.
- 52 M. J. Berger, J. H. Hubbell, S. M. Seltzer, J. Chang, J. S. Coursey, R. Sukumar, D. S. Zucker and K. Olsen, 2010.
- 53 J. A. Lake, *Acta Cryst*, 1967, **23**, 191–194.
- 54 N. Shimizu, T. Mori, Y. Nagatani, H. Ohta, S. Saijo, H. Takagi, M. Takahashi, K. Yatabe, T. Kosuge and N. Igarashi, *AIP Conference Proceedings*, 2019, **2054**, 060041.
- 55 H. Ohgi, H. Imamura, K. Yonenaga, T. Morita, K. Nishikawa, P. Westh and Y. Koga, *J. Mol. Liq.*, 2016, **224**, 401–407.
- 56 H. E. Stanley, *Introduction to Phase Transitions and Critical Phenomena*, New York, 1971.
- 57 Y. Koga, *Solution Thermodynamics and its Application to Aqueous Solutions*, Elsevier, Amsterdam, 2nd edn. 2017.
- 58 H. Hayashi, K. Nishikawa and T. Iijima, *J. Appl. Crystallogr.*, 1990, **23**, 134–135.
- 59 S. Matsuo, R. Yamamoto, H. Kubota and Y. Tanaka, *Int J Thermophys*, 1994, **15**, 245–259.
- 60 M. J. Blandamer, J. Burgess, A. Cooney, H. J. Cowles, I. M. Horn, K. J. Martin, K. W. Morcom and P. Warrick, *J. Chem. Soc. Faraday Trans.*, 1990, **86**, 2209–2213.
- 61 R. Chitra and P. E. Smith, *J. Phys. Chem. B*, 2002, **106**, 1491–1500.
- 62 The Anaesthetic Structure Database (<http://asd.molfield.org>), Database Version: 1.09.9.
- 63 C. F. Anderson, E. S. Courtenay and M. T. Record, *J. Phys. Chem. B*, 2002, **106**, 418–433.
- 64 J. M. Schurr, D. P. Rangel and S. R. Aragon, *Biophys. J.*, 2005, **89**, 2258–2276.
- 65 T. Sumi, Y. Maruyama, A. Mitsutake, K. Mochizuki and K. Koga, *J. Comput. Chem.*, 2018, **39**, 202–217.
- 66 T. Sumi and K. Koga, *Sci. Rep.*, 2019, **9**, 5186.
- 67 B. H. Zimm and J. K. Bragg, *J. Chem. Phys.*, 1959, **31**, 526–535.
- 68 J. Vymětal and J. Vondrášek, *J. Phys. Chem. B*, 2014, **118**, 10390–10404.
- 69 Y. Koga, *Phys. Chem. Chem. Phys.*, 2013, **15**, 14548–14565.
- 70 G. C. Benson and O. Kiyohara, *J. Sol. Chem.*, 1980, **9**, 791–804.
- 71 K. Nakanishi, *Bull. Chem. Soc. Jpn.*, 1960, **33**, 793–797.